JACS
JOURNAL OF THE AMERICAN CHEMICAL SOCIETY
pubs.acs.org/JACS
Communication

# Phosphodianion Activation of Enzymes for Catalysis of Central Metabolic Reactions

Patrick L. Fernandez, Richard W. Nagorski, Judith R. Cristobal, Tina L. Amyes, and John P. Richard*

Cite This: J. Am. Chem. Soc. 2021, 143, 2694–2698
Read Online



**ABSTRACT:** The activation barriers $\Delta G^{\ddagger}$ for $k_{cat}/K_m$ for the reactions of whole substrates catalyzed by 6-phosphogluconate dehydrogenase, glucose 6-phosphate dehydrogenase, and glucose 6-phosphate isomerase are reduced by 11−13 kcal/mol by interactions between the protein and the substrate phosphodianion. Between 4 and 6 kcal/mol of this dianion binding energy is expressed at the transition state for phosphite dianion activation of the respective enzyme-catalyzed reactions of truncated substrates D-xylonate or D-xylose. These and earlier results from studies on $\beta$-phosphoglucomutase, triosephosphate isomerase, and glycerol 3-phosphate dehydrogenase define a cluster of six enzymes that catalyze reactions in glycolysis or of glycolytic intermediates, and which utilize substrate dianion binding energy for enzyme activation. Dianion-driven conformational changes, which convert flexible open proteins to tight protein cages for the phosphorylated substrate, have been thoroughly documented for five of these six enzymes. The clustering of metabolic enzymes which couple phosphodianion-driven conformational changes to enzyme activation suggests that this catalytic motif has been widely propagated in the proteome.

A 12 kcal/mol intrinsic binding energy (IBE)[1] is observed for the substrate phosphodianion in reactions catalyzed by triosephosphate isomerase (TIM)[2−4] and glycerol 3-phosphate dehydrogenase (GPDH),[5,6] where <50% of the 12 kcal/mol dianion binding energy is expressed at the Michaelis complex and >50% is specifically expressed at the transition state for activation of the reaction of a phosphodianion-truncated substrate by a phosphite dianion.[6−8] $\beta$-Phosphoglucomutase (PGM) likewise utilizes the binding energy of the phosphite dianion to produce a 30 000-fold activation of the enzyme for transfer of a covalent phosphoryl reaction intermediate to the anomeric hydroxyl of $\beta$-D-xylopyranose.[9]

Glucose 6-phosphate (G6P) and 6-phosphogluconate (6PG) feature as substrates in the following reactions from Scheme 1: aldose−ketose isomerization catalyzed by glucose 6-phosphate isomerase (PGI),[10] hydride transfer catalyzed by glucose 6-phosphate dehydrogenase (G6PDH),[11] and oxidative decarboxylation catalyzed by 6-phosphogluconate dehydrogenase (6PGDH).[12−14] We report that (i) D-xylose and D-xylonate are poor substrates for catalysis by PGI and G6PDH or by 6PGDH, respectively; (ii) the phosphodianion of whole G6P or 6-phosphogluconate substrates provides ≥11 kcal/mol stabilization of the respective enzymatic transition states; and (iii) between 30 and 50% of this total dianion binding energy is recovered as $HPO_3^{2-}$ activation of the enzyme-catalyzed reactions of phosphodianion-truncated substrates D-xylose (PGI and G6PDH) or D-xylonate (6PGDH). The utilization of dianion binding interactions in catalysis by this tight cluster of six enzymes (Scheme 1), which function at ancient metabolic pathways,[15,16] provides evidence that large phosphodianion and phosphite binding energies are intrinsic to a catalytic motif that appeared early in evolution and which was propagated to glycolytic enzymes and enzymes that pivot intermediates of glycolysis toward the production of pentose phosphates or lipids (Scheme 1).

**Scheme 1. Enzymes with Transition States Strongly Stabilized by Interactions to the Substrate Phosphodianion or Phosphite Dianion**[a]

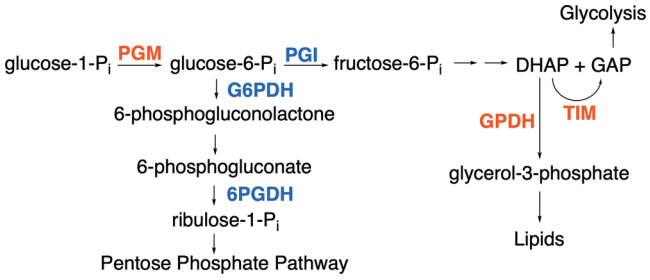


[a]Red: earlier work;[6,9] blue, this work.

The sources for the chemicals and enzymes used in these studies are reported in the Supporting Information (SI). *Ec*6PGDH from *Escherichia coli*, *Lm*G6PDH from *Leuconostoc mesenteroides*, and *Sc*PGI from *Saccharomyces cerevisiae* were shown to each give a single major band by sodium dodecyl sulfate polyacrylamide gel electrophoresis (Figure S1). The experimental protocols for the following enzyme assays are described in the SI: *Ec*6PGDH-, *Lm*G6PDH-, and *Sc*PGI-catalyzed reactions of physiological substrates; the oxidative

Received: December 29, 2020
Published: February 9, 2021





https://dx.doi.org/10.1021/jacs.0c13423
J. Am. Chem. Soc. 2021, 143, 2694−2698

**Scheme 2. Reactions of Whole $[(k_{cat}/K_m)_{SPi}]$ and Truncated $[(k_{cat}/K_m)_S]$ Substrates, and $HPO_3^{2-}$-Activated Reactions of Truncated Substrates $(k_{cat}/K_{Xyl}K_{HPi})$ Catalyzed by (A) *Ec*6PGDH, (B) *Lm*G6PDH, and (C) *Sc*PGI**

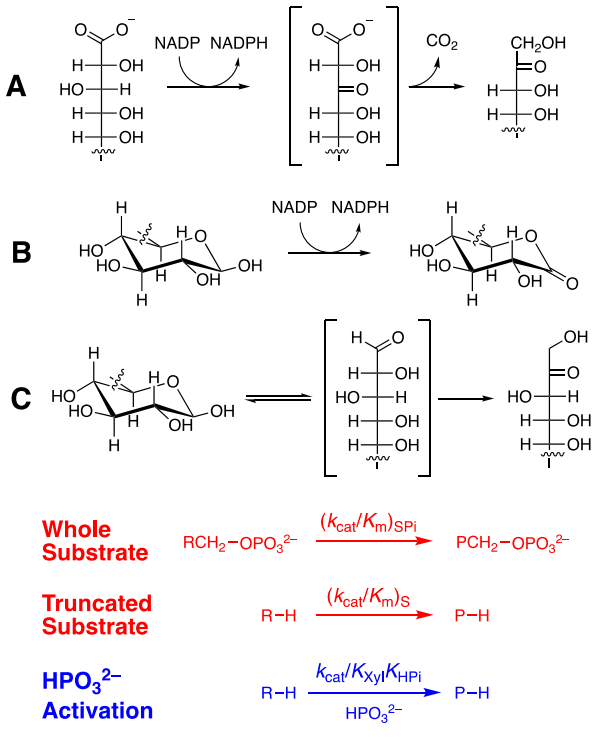


decarboxylation of D-xylonate catalyzed by *Ec*6PGDH; and *Lm*G6PDH-catalyzed oxidation of D-xylose. The *Sc*PGI-catalyzed isomerization of D-xylose (Scheme 2) was monitored by coupling formation of the product D-xylulose to oxidation of NADH catalyzed by sorbitol dehydrogenase.[17]

Figure S2A–C shows Michaelis–Menten plots of $v/[E]$ against [6PG], [G6P], and [F6P], respectively, for the reactions catalyzed by *Ec*6PGDH, *Lm*G6PDH, and *Sc*PGI. These plots give the values of $(k_{cat}/K_m)_{SPi}$ for reactions of whole substrates reported in Table 1, where $(k_{cat}/K_m)_{SPi}$ for the *Sc*PGI-catalyzed reaction of G6P was calculated from $k_{cat}/K_m = 2.38 \times 10^6\ M^{-1}\ s^{-1}$ for isomerization of F6P to form G6P and $K_{eq} = 3.45$ for this isomerization reaction.[19] Figure S3A–C shows plots of $v/[E]$ against [D-xylonate] and [D-xylose] for reactions catalyzed by *Ec*6PGDH (D-xylonate), *Lm*G6PDH (D-xylose), and *Sc*PGI (D-xylose). The slopes of the linear correlations from Figure S3A,B are equal to $(k_{cat}/K_m)_S$ for the reaction of the truncated substrates. Values of $(k_{cat})_S = 0.0047\ s^{-1}$ and $(k_{cat}/K_m)_S = 3.6 \times 10^{-4}\ M^{-1}\ s^{-1}$ (Table 1) were determined from the fit of data from Figure S3C to the Michaelis–Menten equation. The contribution of dianion binding interactions to transition-state stabilization, $(\Delta G^{\ddagger})_{Pi} = RT \ln[(k_{cat}/K_m)_{SPi}/(k_{cat}/K_m)_S]$, are reported in Table 1.[1]

The *Ec*6PGDH-, *Lm*G6PDH-, and *Sc*PGI-catalyzed reactions of dianion-truncated substrates are strongly activated by phosphite dianion. Note that only *Ec*6PGDH-catalyzed oxidation of D-xylonate by NADP was monitored. We have not determined if this enzyme catalyzes the subsequent decarboxylation reaction. We first fit plots of $v/[E]$ against $[HPO_3^{2-}]$ to the full rate equation for Scheme 3 (not shown). However, the uncertainties in the kinetic parameters obtained from these fits (not shown) range from 25 to 100%, because the data do not clearly define the value for $K_{Xyl}$ for weakly bound D-xylose or D-xylonate ($K_{xyl} \gg$ [Xyl], Scheme 3). We

**Scheme 3. Activation of the Catalyzed Reactions of D-Xylonate (*Ec*6PGDH) or D-Xylose (*Lm*G6PDH and *Sc*PGI) by $HPO_3^{2-}$[a]**

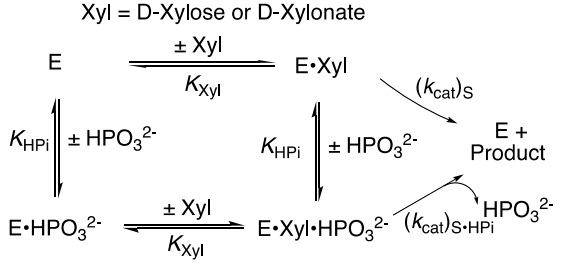


[a]The cofactor NADP is bound to *Lm*G6PDH and *Ec*6PGDH and is reduced to NADPH for the enzyme-catalyzed reactions of D-xylose or D-xylonate.

**Table 1. Kinetic Parameters at pH 7.5 and 25 °C for Enzyme-Catalyzed Reactions of Whole and Phosphodianion Truncated Substrates (Scheme 2), the Total Phosphodianion Binding Energies, and the Dianion Binding Energy Utilized for Enzyme Activation**

| enzyme | $(k_{cat}/K_m)_{SPi}$ $(M^{-1}\ s^{-1})$[e,f] | $(k_{cat}/K_m)_S$ $(M^{-1}\ s^{-1})$[e,f] | $\left(\frac{(k_{cat}/K_{Xyl})_{S\cdot HPi}}{K_{HPi}}\right)$ $(M^{-2}\ s^{-1})$[f,g] | $(\Delta G^{\ddagger})_{Pi}$ (kcal/mol),[h,j] $[IBE]_T$ | $\Delta G^{\ddagger}_{HPi}$ (kcal/mol),[i,j] $[IBE]_{HPi}$ | $[IBE]_{HPi}/[IBE]_T$ |
|---|---|---|---|---|---|---|
| *Sc*PGI[a] | $(6.9 \pm 0.2) \times 10^5$ $k_{cat} = 400\ s^{-1}$ | $(3.6 \pm 0.2) \times 10^{-4}$ | 0.52 ± 0.10 | 12.6 ± 0.1 | 4.3 ± 0.1 | 0.34 |
| *Lm*G6PDH[a] | $(2.0 \pm 0.2) \times 10^6$ $k_{cat} = 320\ s^{-1}$ | $(8.3 \pm 0.1) \times 10^{-3}$ | 53.0 ± 0.3 | 11.4 ± 0.1 | 5.2 ± 0.1 | 0.46 |
| *Ec*6PGDH[b] | $(8.4 \pm 0.4) \times 10^5$ $k_{cat} = 12\ s^{-1}$ | $(9.9 \pm 0.2) \times 10^{-3}$ | 140 ± 1 | 10.8 ± 0.1 | 5.7 ± 0.1 | 0.53 |
| OMPDC[c] | $1.1 \times 10^7$ | 0.026 | 12000 | 11.7 ± 0.1 | 7.7 ± 0.1 | 0.66 |
| TIM[d] | $2.2 \times 10^8$ | 0.062 | 2700 | 13.0 ± 0.1 | 6.3 ± 0.1 | 0.48 |
| GPDH[d] | $4.6 \times 10^6$ | 0.050 | 16000 | 10.8 ± 0.1 | 7.5 ± 0.1 | 0.69 |

[a]SPi = G6P; S = D-xylose. [b]SPi = 6-PG; S = D-xylonate. [c]SPi = orotidine 5′-monophosphate (OMP); S = 1-(β-D-erythrofuranosyl)orotic acid.[6,18] [d]$SP_i$ = dihydroxyacetone phosphate; S = glycolaldehyde.[2,6] [e]Kinetic data for the catalyzed reactions of whole or truncated substrate (see SI). [f]The quoted uncertainty is the standard error obtained from the least-squares fit of experimental data to the appropriate kinetic equation. [g]Third-order rate constant for the phosphite dianion-activated reaction of truncated substrate (Scheme 3). [h]$(\Delta G^{\ddagger})_{Pi} = RT \ln[(k_{cat}/K_m)_{SPi}/(k_{cat}/K_m)_S]$. [i]See eq 3. [j]The approximate uncertainties are calculated from the standard errors in the kinetic parameters.



https://dx.doi.org/10.1021/jacs.0c13423
J. Am. Chem. Soc. 2021, 143, 2694–2698

report these data (Figure 1A–C) as plots of $(v - v_0)/[E]$ against $[HPO_3^{2-}]$ for *Ec*6PGDH-, *Lm*G6PDH-, and *Sc*PGI-

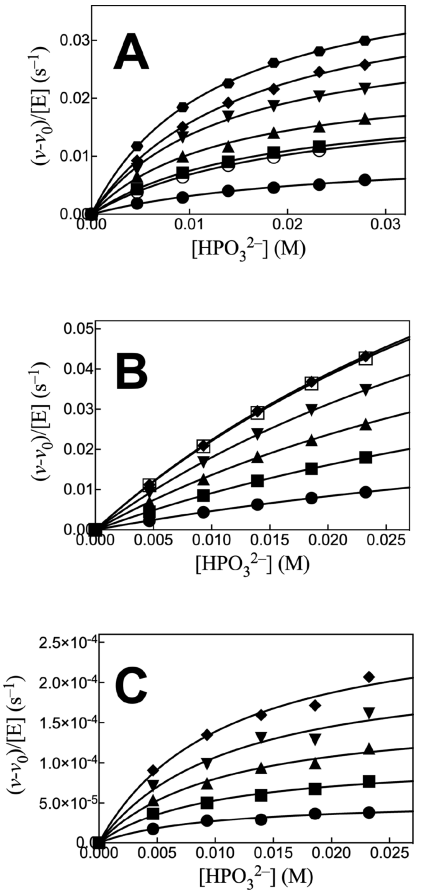


**Figure 1.** Effect of increasing $[HPO_3^{2-}]$ on $(v - v_0)/[E]$ for (A) *Ec*6PGDH-catalyzed reactions of D-xylonate and (B and C) *Lm*G6PDH- and *Sc*PGI-catalyzed reactions of D-xylose, respectively. (A) Reactions at the following [D-xylonate]: 4.1, 10, 12.4, 16.5, 20, and 24 mM. (B and C) Reactions at the following [D-xylose]: 10, 20, 30, 40, and 50 mM. The solid and open symbols for panels A (10 mM D-xylonate) and B (50 mM D-xylose) show data for reactions at 1.0 and 0.5 mM NADP, respectively.

catalyzed reactions at different fixed concentrations of D-xylonate (1A) or D-xylose (1B and 1C), where $(v - v_0)$ is the difference in the initial velocity for reactions in the presence and absence of $HPO_3^{2-}$. The $HPO_3^{2-}$-activated reactions of *Ec*6PGDH and *Lm*G6PDH were carried out at saturating [NADP] = 1 mM. Data from Figure 1 show that essentially the same enzyme activation is observed for reactions at 0.5 mM (open symbols) and 1.0 mM (solid symbols) [NADP]. The solid lines from Figure 1A–C show the fits of these kinetic data to eq 1, derived for Scheme 3, with the assumption that $K_{Xyl} \gg [Xyl]$ and using the derived values of $(k_{cat}/K_{HPi})_{obs}$ (eq 2).

$$\frac{v - v_0}{[E]} = \frac{(k_{cat})_{S\cdot HPi}[HPO_3^{2-}][Xyl]}{K_{Xyl}K_{HPi} + K_{Xyl}[HPO_3^{2-}]} \quad (1)$$

$$(k_{cat}/K_{HPi})_{obs} = \frac{(k_{cat})_{S\cdot HPi}[Xyl]}{K_{Xyl}K_{HPi}} \quad (2)$$

Figure 2A shows plots of $(k_{cat}/K_{HPi})_{obs}$, determined for the corresponding plots from Figure 1, against [Xyl] for the

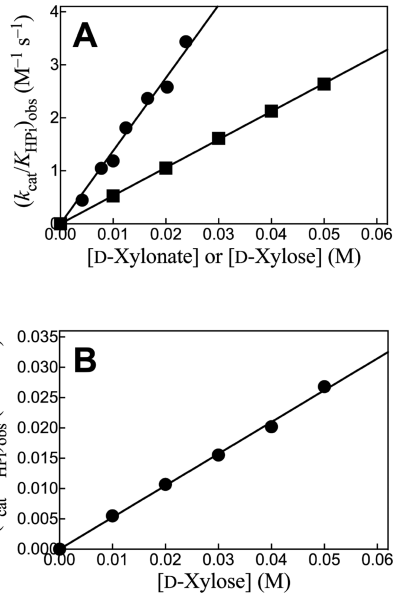


**Figure 2.** Effect of increasing [D-xylonate] or [D-xylose] on $(k_{cat}/K_{HPi})_{obs}$ for dianion activation of the catalyzed reactions of truncated substrates (Scheme 3). (A) *Ec*6PGDH-catalyzed reactions of D-xylonate (●) and *Lm*G6PDH-catalyzed oxidation of D-xylose by NADP (■). (B) *Sc*PGI-catalyzed isomerization of D-xylose (●).

reactions catalyzed by *Ec*6PGDH and *Lm*G6PDH, while Figure 2B shows a similar plot for reactions catalyzed by *Sc*PGI. The slopes, $(k_{cat})_{S\bullet HPi}/K_{Xyl}K_{HPi}$ (eq 2), for these linear plots are reported in Table 1. The absence of detectable curvature for plots from Figure 2 shows that $K_{Xyl}K_{HPi} \gg K_{Xyl}[HPO_3^{2-}]$ (eq 1), and that there is no significant accumulation of ternary $[E\cdot Xyl\cdot HPO_3^{2-}]$ complexes. By contrast, robust binding of phosphorylated substrates is observed ($K_m$ = 10–100 $\mu$M, SI) because of the entropic advantage to reactions of the whole substrates compared with the corresponding substrate pieces.[18,20,21]

Table 1 also reports (1) the total transition-state stabilization from binding interactions with phosphite dianion (intrinsic binding energy $[IBE]_{HPi}$), calculated from eq 3

$$\Delta G^{\ddagger}_{HPi} = -RT \ln K^{\ddagger}_{HPi} = \frac{K_{HPi}(k_{cat}/K_{Xyl})_S}{(k_{cat}/K_{Xyl})_{S\cdot HPi}} \quad (3)$$

derived for Scheme 4; (2) the fraction $([IBE]_{HPi}/[IBE]_T)$ of the total intrinsic phosphodianion binding energy $[IBE]_T$ that is expressed at the transition state for the phosphite dianion-activated reaction of truncated substrate (Scheme 4); and (3)

**Scheme 4. Ground-State ($K_{HPi}$) and Transition-State ($K^{\ddagger}_{HPi}$]) Binding of $HPO_3^{2-}$ to *Ec*6PGDH, *Lm*G6PDH, and *Sc*PGI**

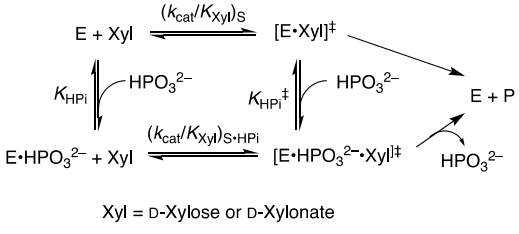




https://dx.doi.org/10.1021/jacs.0c13423
J. Am. Chem. Soc. 2021, 143, 2694–2698

the corresponding kinetic parameters determined for isomerization, decarboxylation, and hydride-transfer reactions catalyzed by TIM, orotidine 5′-monophosphate decarboxylase (OMPDC), and GPDH, respectively.[2,5,6,18] *Sc*PGI catalyzes both ring-opening of cyclic sugar phosphates and subsequent isomerization of the acyclic sugar,[22] while *Ec*6PGDH catalyzes the coupled hydride-transfer and decarboxylation reactions of 6PG. We have not determined the transition-state stabilization for the individual enzymatic reaction steps from interactions with the substrate phosphodianion or phosphite dianion piece. We note earlier reports of phosphite dianion activation of both enzyme-catalyzed hydride transfer[5,23,24] and decarboxylation reaction[18] of phosphodianion-truncated substrates.

The data from Table 1 and from an earlier study on catalysis by PGM[9] define a cluster of six metabolic enzymes (Scheme 1) that show strong activation by $HPO_3^{2-}$ for the catalytic turnover of substrates, D-xylose, D-xylonate, or glycolaldehyde. *Ec*6PGDH, *Lm*G6PDH, and *Sc*PGI show smaller values of $k_{cat}/K_m$ for the catalyzed reactions of both whole and truncated substrates, compared with the corresponding kinetic parameters for the TIM- and GPDH-catalyzed reactions of dihydroxyacetone phosphate and glycolaldehyde substrates. However, similar total intrinsic phosphodianion binding energies of 11−13 kcal/mol are observed for these five enzymes and for OMPDC (Table 1). Apparently, 13 kcal/mol, which corresponds to a $>10^{10}$-fold rate acceleration, represents an operational limit for transition-state stabilization from catalytic protein−dianion interactions. A larger fraction of the total dianion binding energy, ≤70% compared with ≤50%, is recovered in the activation of reactions of glycolaldehyde compared with D-xylonate or D-xylose by $HPO_3^{2-}$. This corresponds to a larger specificity in the utilization of $HPO_3^{2-}$ binding energy for the ground state relative to the transition state in enzymes that catalyze the reactions of 6-carbon versus 3-carbon substrates.[7,25]

We have proposed a model for enzyme activation in which unliganded catalysts exist in flexible, open, but inactive conformations, and protein−dianion interactions are utilized to stabilize a fully active, rigid, and closed enzyme.[3,25] This model is supported by the results from experimental and computational studies on TIM,[20,26,27] OMPDC,[28,29] and GPDH.[30,31] It provides a rationalization for dianion activation of reactions catalyzed by 6PGDH[14] and PGI[32] because substrate binding to these enzymes gives rise to sizable phosphodianion-driven conformational changes. It may hold for catalysis by G6PDH; however, we are not aware of X-ray crystal structures for G6PDH which show the bound cofactor and substrate positioned to undergo hydride transfer.

Evolutionary pressure to optimize energy production from nutrients has driven TIM to perfection in catalysis of the isomerization of triosephosphate.[33] This catalytic perfection is presumably reflected in the structure for the iconic TIM barrel.[34] We propose that enzyme catalysis, with utilization of phosphodianion binding energy to drive an enzyme-activating conformational change, appeared early in protein evolution and that this powerful catalytic motif has been replicated in the evolution of metabolic pathways (Scheme 1) and of enzymes that serve a host of cellular functions.

## ■ ASSOCIATED CONTENT

### Supporting Information

The Supporting Information is available free of charge at https://pubs.acs.org/doi/10.1021/jacs.0c13423.

Experimental Section with (i) the sources of the enzymes and chemicals used in this work; (ii) experimental protocol for the determination of kinetic parameters for whole substrate and the substrate pieces; (iii) Figure S1 showing the SDS-PAGE gel of the commercial enzymes *Ec*6PGDH, *Lm*G6PDH, *Sc*PGI, and sorbitol dehydrogenase used in these studies; and (iv) figures with kinetic data for enzyme-catalyzed reactions of the whole substrate (Figure S2) and the phosphodianion-truncated substrate piece (Figure S3) (PDF)

## ■ AUTHOR INFORMATION


### Corresponding Author

**John P. Richard** − *Department of Chemistry, University at Buffalo, SUNY, Buffalo, New York 14260-3000, United States;* orcid.org/0000-0002-0440-2387; Email: jrichard@buffalo.edu

### Authors

**Patrick L. Fernandez** − *Department of Chemistry, University at Buffalo, SUNY, Buffalo, New York 14260-3000, United States;* orcid.org/0000-0002-1862-5063

**Richard W. Nagorski** − *Department of Chemistry, Illinois State University, Normal, Illinois 61790-4160, United States;* orcid.org/0000-0002-0769-9972

**Judith R. Cristobal** − *Department of Chemistry, University at Buffalo, SUNY, Buffalo, New York 14260-3000, United States*

**Tina L. Amyes** − *Department of Chemistry, University at Buffalo, SUNY, Buffalo, New York 14260-3000, United States*

Complete contact information is available at: https://pubs.acs.org/10.1021/jacs.0c13423



### Funding

The authors acknowledge the National Institutes of Health Grant GM134881 for support of this work.


### Notes

The authors declare no competing financial interest.

## ■ ABBREVIATIONS

IBE, intrinsic binding energy; TIM, triosephosphate isomerase; GPDH, glycerol 3-phosphate dehydrogenase; PGM, β-phosphoglucomutase; G6P, glucose 6-phosphate; 6PG, 6-phosphogluconate; PGI, glucose 6-phosphate isomerase; G6PDH, glucose 6- phosphate dehydrogenase; 6PGDH, 6-phosphogluconate dehydrogenase; *Ec*6PGDH, 6-phosphogluconate dehydrogenase from *Escherichia coli*; *Lm*G6PDH, glucose 6-phosphate dehydrogenase from *Leuconostoc mesenteroides*; OMPDC, orotidine 5′-monophosphate decarboxylase; *Sc*PGI, glucose 6-phosphate isomerase from *Saccharomyces cerevisiae*

## ■ REFERENCES


(1) Jencks, W. P. Binding energy, specificity, and enzymic catalysis: the Circe effect. *Adv. Enzymol. Relat. Areas Mol. Biol.* **2006**, *43*, 219−410.

(2) Amyes, T. L.; Richard, J. P. Enzymatic catalysis of proton transfer at carbon: activation of triosephosphate isomerase by phosphite dianion. *Biochemistry* **2007**, *46*, 5841−5854.

(3) Go, M. K.; Amyes, T. L.; Richard, J. P. Hydron Transfer Catalyzed by Triosephosphate Isomerase. Products of the Direct and

Phosphite-Activated Isomerization of [1-$^{13}$C]-Glycolaldehyde in $D_2O$. *Biochemistry* **2009**, *48*, 5769−5778.
(4) Amyes, T. L.; O'Donoghue, A. C.; Richard, J. P. Contribution of phosphate intrinsic binding energy to the enzymatic rate acceleration for triosephosphate isomerase. *J. Am. Chem. Soc.* **2001**, *123*, 11325−11326.
(5) Tsang, W.-Y.; Amyes, T. L.; Richard, J. P. A Substrate in Pieces: Allosteric Activation of Glycerol 3-Phosphate Dehydrogenase ($NAD^+$) by Phosphite Dianion. *Biochemistry* **2008**, *47*, 4575−4582.
(6) Reyes, A. C.; Zhai, X.; Morgan, K. T.; Reinhardt, C. J.; Amyes, T. L.; Richard, J. P. The Activating Oxydianion Binding Domain for Enzyme-Catalyzed Proton Transfer, Hydride Transfer and Decarboxylation: Specificity and Enzyme Architecture. *J. Am. Chem. Soc.* **2015**, *137*, 1372−1382.
(7) Richard, J. P. Protein Flexibility and Stiffness Enable Efficient Enzymatic Catalysis. *J. Am. Chem. Soc.* **2019**, *141*, 3320−3331.
(8) Amyes, T. L.; Malabanan, M. M.; Zhai, X.; Reyes, A. C.; Richard, J. P. Enzyme activation through the utilization of intrinsic dianion binding energy. *Protein Eng., Des. Sel.* **2017**, *30*, 159−168.
(9) Ray, W. J., Jr.; Long, J. W. Thermodynamics and mechanism of the $PO_3$ transfer process in the phosphoglucomutase reaction. *Biochemistry* **1976**, *15*, 3993−4006.
(10) Meng, M.; Lin, H.-Y.; Hsieh, C.-J.; Chen, Y.-T. Functions of the conserved anionic amino acids and those interacting with the substrate phosphate group of phosphoglucose isomerase. *FEBS Lett.* **2001**, *499*, 11−14.
(11) Vought, V.; Ciccone, T.; Davino, M. H.; Fairbairn, L.; Lin, Y.; Cosgrove, M. S.; Adams, M. J.; Levy, H. R. Delineation of the Roles of Amino Acids Involved in the Catalytic Functions of *Leuconostoc mesenteroides* Glucose 6-Phosphate Dehydrogenase. *Biochemistry* **2000**, *39*, 15012−15021.
(12) Rippa, M.; Giovannini, P. P.; Barrett, M. P.; Dallocchio, F.; Hanau, S. 6-Phosphogluconate dehydrogenase: the mechanism of action investigated by a comparison of the enzyme from different species. *Biochim. Biophys. Acta, Protein Struct. Mol. Enzymol.* **1998**, *1429*, 83−92.
(13) Cervellati, C.; Dallocchio, F.; Bergamini, C. M.; Cook, P. F. Role of methionine-13 in the catalytic mechanism of 6-phosphogluconate dehydrogenase from sheep liver. *Biochemistry* **2005**, *44*, 2432−2440.
(14) Chen, Y.-Y.; Ko, T.-P.; Chen, W.-H.; Lo, L.-P.; Lin, C.-H.; Wang, A. H. J. Conformational changes associated with cofactor/substrate binding of 6-phosphogluconate dehydrogenase from *Escherichia coli* and *Klebsiella pneumoniae*: Implications for enzyme mechanism. *J. Struct. Biol.* **2010**, *169*, 25−35.
(15) Fothergill-Gilmore, L. A.; Michels, P. A. M. Evolution of Glycolysis. *Prog. Biophys. Mol. Biol.* **1993**, *59*, 105−235.
(16) Goldman, A. D.; Beatty, J. T.; Landweber, L. F. The TIM Barrel Architecture Facilitated the Early Evolution of Protein-Mediated Metabolism. *J. Mol. Evol.* **2016**, *82*, 17−26.
(17) Toteva, M. M.; Silvaggi, N. R.; Allen, K. N.; Richard, J. P. Binding Energy and Catalysis by D-Xylose Isomerase: Kinetic, Product, and X-ray Crystallographic Analysis of Enzyme-Catalyzed Isomerization of (R)-Glyceraldehyde. *Biochemistry* **2011**, *50*, 10170−10181.
(18) Amyes, T. L.; Richard, J. P.; Tait, J. J. Activation of orotidine 5′-monophosphate decarboxylase by phosphite dianion: The whole substrate is the sum of two parts. *J. Am. Chem. Soc.* **2005**, *127*, 15708−15709.
(19) Tewari, Y. B.; Steckler, D. K.; Goldberg, R. N. Thermodynamics of isomerization reactions involving sugar phosphates. *J. Biol. Chem.* **1988**, *263*, 3664−3669.
(20) Zhai, X.; Amyes, T. L.; Richard, J. P. Enzyme Architecture: Remarkably Similar Transition States for Triosephosphate Isomerase-Catalyzed Reactions of the Whole Substrate and the Substrate in Pieces. *J. Am. Chem. Soc.* **2014**, *136*, 4145−4148.
(21) Jencks, W. P. On the attribution and additivity of binding energies. *Proc. Natl. Acad. Sci. U. S. A.* **1981**, *78*, 4046−50.
(22) Schray, K. J.; Benkovic, S. J.; Benkovic, P. A.; Rose, I. A. Catalytic reactions of phosphoglucose isomerase with cyclic forms of glucose 6-phosphate and fructose 6-phoshate. *J. Biol. Chem.* **1973**, *248*, 2219−24.
(23) Kholodar, S. A.; Allen, C. L.; Gulick, A. M.; Murkin, A. S. The Role of Phosphate in a Multistep Enzymatic Reaction: Reactions of the Substrate and Intermediate in Pieces. *J. Am. Chem. Soc.* **2015**, *137*, 2748−2756.
(24) Kholodar, S. A.; Murkin, A. S. DXP Reductoisomerase: Reaction of the Substrate in Pieces Reveals a Catalytic Role for the Nonreacting Phosphodianion Group. *Biochemistry* **2013**, *52*, 2302−2308.
(25) Amyes, T. L.; Richard, J. P. Specificity in transition state binding: The Pauling model revisited. *Biochemistry* **2013**, *52*, 2021−2035.
(26) Kulkarni, Y. S.; Liao, Q.; Byléhn, F.; Amyes, T. L.; Richard, J. P.; Kamerlin, S. C. L. Role of Ligand-Driven Conformational Changes in Enzyme Catalysis: Modeling the Reactivity of the Catalytic Cage of Triosephosphate Isomerase. *J. Am. Chem. Soc.* **2018**, *140*, 3854−3857.
(27) Zhai, X.; Amyes, T. L.; Richard, J. P. Role of Loop-Clamping Side Chains in Catalysis by Triosephosphate Isomerase. *J. Am. Chem. Soc.* **2015**, *137*, 15185−15197.
(28) Goryanova, B.; Goldman, L. M.; Ming, S.; Amyes, T. L.; Gerlt, J. A.; Richard, J. P. Rate and Equilibrium Constants for an Enzyme Conformational Change during Catalysis by Orotidine 5′-Monophosphate Decarboxylase. *Biochemistry* **2015**, *54*, 4555−4564.
(29) Goldman, L. M.; Amyes, T. L.; Goryanova, B.; Gerlt, J. A.; Richard, J. P. Enzyme Architecture: Deconstruction of the Enzyme-Activating Phosphodianion Interactions of Orotidine 5′-Monophosphate Decarboxylase. *J. Am. Chem. Soc.* **2014**, *136*, 10156−10165.
(30) Mydy, L. S.; Cristobal, J. R.; Katigbak, R. D.; Bauer, P.; Reyes, A. C.; Kamerlin, S. C. L.; Richard, J. P.; Gulick, A. M. Human Glycerol 3-Phosphate Dehydrogenase: X-Ray Crystal Structures that Guide the Interpretation of Mutagenesis Studies. *Biochemistry* **2019**, *58*, 1061−1073.
(31) He, R.; Reyes, A. C.; Amyes, T. L.; Richard, J. P. Enzyme Architecture: The Role of a Flexible Loop in Activation of Glycerol-3-phosphate Dehydrogenase for Catalysis of Hydride Transfer. *Biochemistry* **2018**, *57*, 3227−3236.
(32) Arsenieva, D.; Jeffery, C. J. Conformational Changes in Phosphoglucose Isomerase Induced by Ligand Binding. *J. Mol. Biol.* **2002**, *323*, 77−84.
(33) Knowles, J. R.; Albery, W. J. Perfection in enzyme catalysis: the energetics of triosephosphate isomerase. *Acc. Chem. Res.* **1977**, *10*, 105−111.
(34) Sterner, R.; Hocker, B. Catalytic versatility, stability, and evolution of the $(\beta/\alpha)_8$-barrel enzyme fold. *Chem. Rev.* **2005**, *105*, 4038−4055.


https://dx.doi.org/10.1021/jacs.0c13423
*J. Am. Chem. Soc.* 2021, 143, 2694−2698